Zitierweise: *Angew. Chem. Int. Ed.* **2024**, e202418314
doi.org/10.1002/anie.202418314

Medicinal Chemistry

Expedited SARS-CoV-2 Main Protease Inhibitor Discovery through Modular 'Direct-to-Biology' Screening

*Harry Wilders, George Biggs, Sam M. Rowe, Emma E. Cawood, Ioannis G. Riziotis, Alan R. Rendina, Emma K. Grant, Jonathan Pettinger, David J. Fallon, Mark Skehel, David House, Nicholas C. O. Tomkinson, and Jacob T. Bush**

Abstract: Reactive fragment (RF) screening has emerged as an efficient method for ligand discovery across the proteome, irrespective of a target's perceived tractability. To date, however, the efficiency of subsequent optimisation campaigns has largely been low-throughput, constrained by the need for synthesis and purification of target compounds. We report an efficient platform for 'direct-to-biology' (D2B) screening of cysteine-targeting chloroacetamide RFs, wherein synthesis is performed in 384-well plates allowing direct assessment in downstream biological assays without purification. Here, the developed platform was used to optimise inhibitors of SARS-CoV-2 main protease (M^{Pro}), an established drug target for the treatment of COVID-19. An initial RF hit was developed into a series of potent inhibitors, and further exploration using D2B screening enabled a 'switch' to a reversible inhibitor series. This example of ligand discovery for M^{Pro} illustrates the acceleration that D2B chemistry can offer for optimising RFs towards covalent inhibitor candidates, as well as providing future impetus to explore the evolution of RFs into non-covalent ligands.

Introduction

The emergence of severe acute respiratory coronavirus 2 (SARS-CoV-2) and the resultant COVID-19 pandemic has had a profound impact on human society and health. Large-scale efforts have been conducted to discover and develop potential treatments, resulting in the approval of numerous vaccines, and a clinical pipeline of small molecule therapeutics.[1] Small molecule drug discovery efforts have focussed primarily on inhibiting the two viral proteases (main protease, M^{Pro} and papain-like protease,[2] PL^{Pro}); of these targets, M^{Pro} has received the greater attention. The main protease represents a compelling drug target, due to its low sequence overlap with human proteases, and the essentiality of its function in the SARS-CoV-2 life cycle.[3] M^{Pro} is a cysteine protease with a catalytic cysteine (Cys 145) that participates in the cleavage of large, non-functional polyproteins into the proteins required for viral replication.[4] Numerous M^{Pro} ligands have been reported, encompassing a wide range of medicinal chemistry approaches including proteolysis-targeting chimeras (PROTACs),[5] encoded library technologies,[6] and covalent drug discovery.[7] The sole small molecule approved for the treatment of COVID-19, nirmatrelvir, acts *via* reversible, covalent inhibition of M^{Pro} through modification of the catalytic cysteine.[1a] While nirmatrelvir has successfully been employed for treating COVID-19 in the clinic, its continued use is leading to the emergence of resistance mutations.[8] Furthermore, nirmatrelvir must be administered with the protease inhibitor ritonavir, which limits the number of patients who can receive treatment due to potential drug-drug interactions.[9] Continued development of next-generation inhibitors is therefore required to maintain treatment options for SARS-CoV-2 infections and ensure preparedness for future SARS coronaviruses.

The activity of M^{Pro} is dependent upon the catalytic cysteine, therefore, approaches which covalently modify this cysteine are an attractive therapeutic prospect. An established approach to the rational design of covalent modifiers utilises reactive fragment (RF) screening to discover hit molecules for subsequent drug discovery.[10] RF drug discovery aims to identify highly efficient ligands and can offer

[*] H. Wilders, Dr. S. M. Rowe, Dr. E. K. Grant, Dr. J. Pettinger, Dr. D. J. Fallon, Dr. D. House, Dr. J. T. Bush
Chemical Biology, GSK
Gunnels Wood Road, Stevenage, Hertfordshire, SG1 2NY, UK
E-mail: Jacob.x.bush@gsk.com

H. Wilders, Dr. G. Biggs, Dr. E. E. Cawood, Dr. I. G. Riziotis, Dr. J. Pettinger, Dr. D. House, Dr. J. T. Bush
Crick-GSK Biomedical Linklabs, GSK
Gunnels Wood Road, Stevenage, Hertfordshire, SG1 2NY, UK

H. Wilders, Prof. N. C. O. Tomkinson, Dr. J. T. Bush
Pure and Applied Chemistry
University of Strathclyde
295 Cathedral Street, Glasgow, G1 1XL, UK

Dr. A. R. Rendina
Screening, Profiling and Mechanistic Biology, GSK
1250 South Collegeville Road, Collegevill, PA, 19426, US

Dr. M. Skehel
Proteomics Science Technology Platform
The Francis Crick Institute
1 Midland Road, London, NW1 1AT, UK

exceptional selectivity and increased potency through irreversible binding.[10–11] This provides excellent sensitivity, and captures binding interactions even when reversible affinity is poor. RFs have been leveraged to discover ligands for proteins previously considered 'undruggable' due to the shallow or transient nature of their binding sites, as exemplified by the recent approval of sotorasib to inhibit the KRAS-G12C mutant in non-small cell lung cancers.[12] Screening libraries of 10^2-10^3 RFs has been demonstrated to be an efficient method to identify hits.[13] A challenge in RF drug discovery is the optimisation and progression of weak affinity hits to achieve the potency and selectivity required for a therapeutic. This is particularly poignant for human diseases that require urgent therapeutic interventions, such as COVID-19.

As interest in the rational design of covalent therapeutics increases, new technologies are required to improve the efficiency of the process. Methods that reduce synthetic bottlenecks are particularly appealing and have proven successful in drug discovery.[14] Of particular note are emerging 'direct-to-biology' (D2B) methods, where compounds are synthesised using biologically-compatible chemistry to allow immediate activity assessment without purification. D2B has been effectively applied in accelerating several drug discovery campaigns including anti-infectives,[15] proteolysis-targeting chimeras[16] and molecular glues.[17] Despite the promise of D2B approaches, application within covalent drug discovery remains limited.[12a,18]

Herein we report the development of a D2B platform for cysteine-targeting reactive fragments and its application towards the discovery of potent inhibitors of SARS-CoV-2 M^{Pro}. The platform employs parallel synthesis of 10^2–10^3 fragments with direct integration into downstream biological assays, to enable fast design-make-test cycles for drug discovery campaigns. The platform was applied to the optimisation of a RF hit against M^{Pro} to deliver multiple inhibitors with nanomolar potency. The most potent inhibitor was found to engage the catalytic cysteine of M^{Pro} in cells with good selectivity, and also showed engagement of an M^{Pro} mutant that is known to cause resistance to nirmatrelvir, providing a potential opportunity for development of next-generation M^{Pro} inhibitors. We subsequently demonstrate the reactivity of the chloroacetamide electrophile can be tuned to reduce the intrinsic reactivity of the inhibitor without ablating M^{Pro} inhibition. Finally, the D2B approach was applied to the development of non-covalent inhibitors of M^{Pro} based upon the pharmacophores discovered in RF screening. Considered together, this D2B platform represents a powerful approach for RF hit optimisation, enabling both covalent and non-covalent drug discovery.

Results and Discussion

Identification Of Irreversible Inhibitors Targeting SARS-CoV-2 M^{Pro}

SARS-CoV-2 M^{Pro} was initially screened against a library of 219 purified chloroacetamide RFs to identify covalent hits as starting points for further optimisation. The library was designed to include diverse pharmacophores and be 'rule-of-three' compliant (Figure S1).[19] Screening was conducted by incubating M^{Pro} (0.5 μM) with RFs (5 μM) at 4 °C for 16 hours, employing intact-protein liquid chromatography mass spectrometry (IP-LC/MS) to determine the extent of covalent labelling for each fragment molecule.[20] Covalent labelling was quantified by comparing the relative intensities of apo protein and protein-fragment adducts (Figure 1).[21] Six fragments surpassed a hit-calling threshold of 75 % covalent labelling, representing a 2.7 % hit-rate (Figure 1). All six fragments resulted in a single labelling event with the correct expected mass of modification (Apo + Fragment-HCl, Figure S2). Some early structure-activity relationships (SAR) were observed in these hits, such as the presence of indole substructures (**1** and **4**), and morpholine or morpholine bioisosteres (**2**, **5** and **6**) (Figure 1).

To investigate the functional impact of reactive fragment binding, the inhibitory potency of compounds **1**–**6** was determined *via* an enzymatic assay. A fluorogenic M^{Pro} substrate peptide was employed, which upon proteolytic cleavage resulted in separation of a FRET-quench pair, increasing fluorescence intensity.[22] To measure the inhibition of M^{Pro} by the identified fragments, the protein was incubated with hits (1.3–50 μM) and the fluorogenic peptide (40 μM), and the relative fluorescence intensity measured over time. The half-maximal inhibitory potency (IC_{50}) was determined following a one-hour incubation of the fragment and M^{Pro} (Figure 1D). Although all six fragments labelled M^{Pro} to comparable extents (79–97 %), they exhibited more than a log-fold range in inhibitory potency (pIC_{50} (1 h) = 4.5–5.9). Two fragments resulted in an IC_{50} less than 10 μM ($pIC_{50} > 5$), with compound **2** exhibiting the most potent inhibition ($pIC_{50} = 5.9 \pm 0.5$). Owing to the time-dependent nature of irreversible inhibition, a more appropriate measure of potency is the second-order rate constant of inhibition (k_{inact}/K_I).[23] This parameter was determined for compounds **1**–**6** by measuring the observed rate of inhibition (k_{obs}) at five concentrations of fragment, with the slope of the resultant linear regression providing k_{inact}/K_I (Figure 1E). A range of potencies were determined (k_{inact}/K_I = 22–170 $M^{-1}\,s^{-1}$), with compound **2** yielding the fastest rate of covalent inhibition, aligning with the half-maximal inhibitory potency observed.

Measurement of the intrinsic reactivity of covalent inhibitors is essential to understand the likelihood of off-target engagement.[24] The intrinsic reactivity of compounds **1**–**6** was measured as the half-life of the fragment in the presence of an excess of glutathione, a commonly used cysteine-containing tripeptide.[25] To provide a benchmark for reactivity, osimertinib (a recently approved covalent EGFR inhibitor)[26] was adopted as a standard, with a

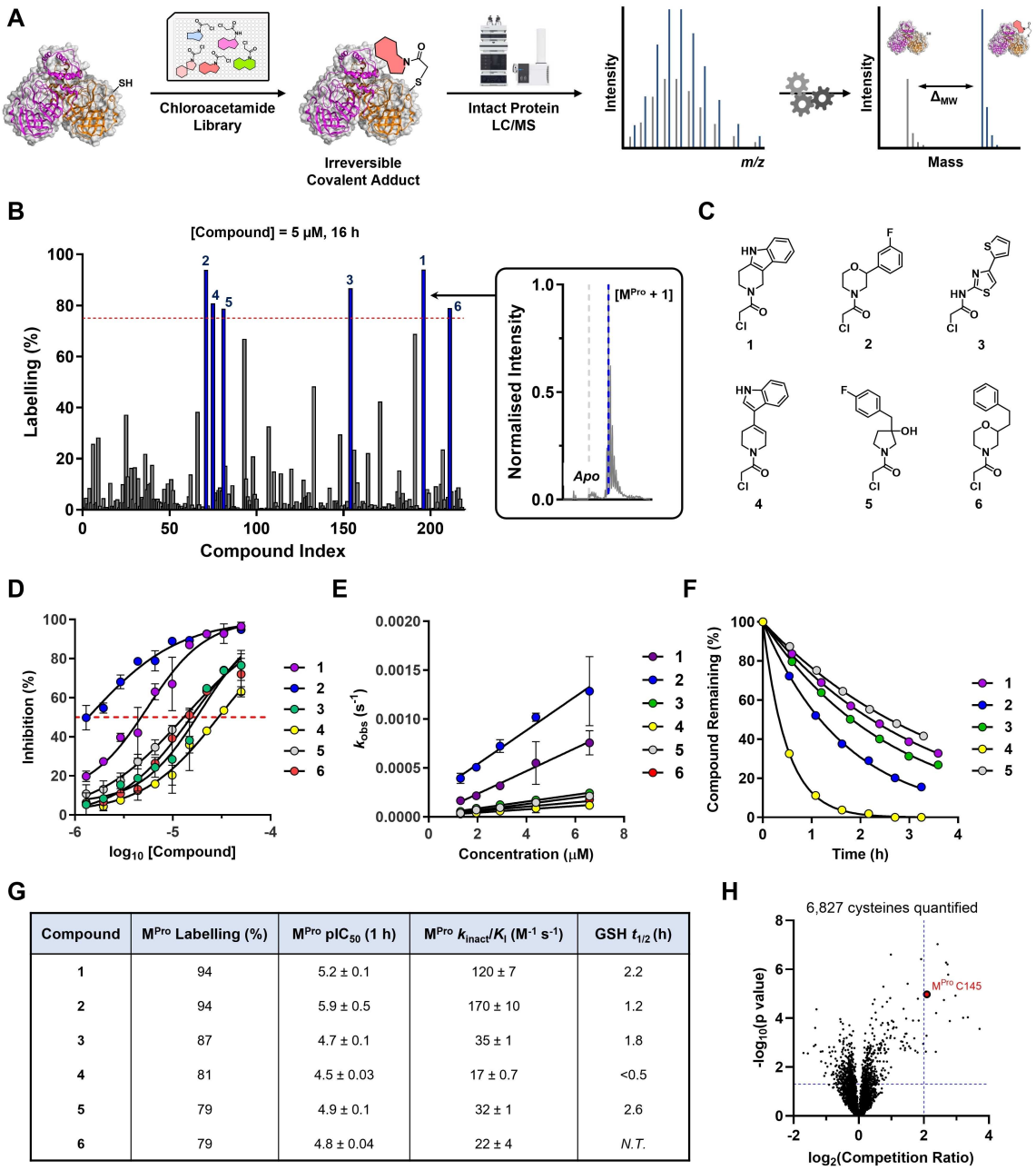

Compound	M^{Pro} Labelling (%)	M^{Pro} pIC$_{50}$ (1 h)	M^{Pro} k_{inact}/K_I (M^{-1} s^{-1})	GSH $t_{1/2}$ (h)
1	94	5.2 ± 0.1	120 ± 7	2.2
2	94	5.9 ± 0.5	170 ± 10	1.2
3	87	4.7 ± 0.1	35 ± 1	1.8
4	81	4.5 ± 0.03	17 ± 0.7	<0.5
5	79	4.9 ± 0.1	32 ± 1	2.6
6	79	4.8 ± 0.04	22 ± 4	*N.T.*

Figure 1. Hit discovery against SARS-CoV-2 M^{Pro} by chloroacetamide reactive fragment screening. (A) A schematic demonstrating the intact-protein mass spectrometry (IP-LC/MS) assay utilised for identifying irreversible ligands to M^{Pro}. A library of 219 chloroacetamides were screened (5 µM, 16 h, 4 °C) and analysed via IP-LC/MS. The extent of covalent modification was quantified from the intensity of the deconvoluted mass spectrum. Formation of the desired fragment-M^{Pro} adduct was ensured by calculating the Δ_{MW} of the observed M^{Pro} species. (B) The extent of covalent labelling for the 219-membered chloroacetamide library as determined by IP-LC/MS. A threshold of 75 % labelling was applied to identify hits. A representative IP-LC/MS trace is shown for hit fragment **1**. (C) The structures of the six hit chloroacetamide reactive fragments identified. (D) The concentration dependent inhibition of M^{Pro} activity following a one-hour incubation for the six hit chloroacetamides. Fragments were incubated with M^{Pro} and a fluorogenic substrate in duplicate, with the rate of substrate turnover employed to measure M^{Pro} activity. A log(inhibitor) vs. response four parameter variable slope model was used to fit curves. Error bars show the standard deviation across replicates. (E) The concentration dependence on the observed rate (k_{obs}) of M^{Pro} activity for each hit fragment. The concentration range screened ensured linearity between concentration and k_{obs}, such that the second-order rate constant of covalent inhibition (k_{inact}/K_I) for each fragment could be calculated. Error bars show the standard deviation across duplicates. (F) The time-dependent loss of each hit fragment in the presence of an excess of glutathione. The half-life of the fragment was used as a measure of the intrinsic reactivity of the electrophile. (G) A table compiling the obtained biophysical and biochemical data for the six identified hit fragments. (H) A volcano plot denoting the mean log$_2$-transformed competition ratio (CR) and associated -log$_{10}$-transformed p-value for each detected cysteine across four technical replicates of compound **2** and DMSO treatments. Calculated *p*-values were derived from the Welch's unpaired t-test. A significance threshold of $p < 0.05$, corresponding to a -log$_{10}$ *p*-value > 1.3, and a CR > 4, corresponding to a log$_2$ CR > 2, was selected. The detected peptide corresponding to M^{Pro} Cys145 has been highlighted.

determined half-life of 1.3 hours (Figure S3). Compounds **1**, **2**, **3** and **5** all exhibited half-lives comparable or greater than that of osimertinib, while compound **4** was found to be more reactive ($t_{1/2}$ < 0.5 h). The stability of compounds **1**, **2**, **3** and **5** was surprising given the chloroacetamide electrophile is typically considered more reactive than an acrylamide (present in osimertinib).[27] Compound **2** was selected for further optimisation due to its superior potency against M^{Pro} among the identified hit fragments along with its suitable reactivity.

Prior to undertaking further optimisation, compound **2** was assessed for engagement of M^{Pro} in live cells by chemoproteomics. Live A549 cells, transduced to express full-length M^{Pro} with a baculovirus vector (Figure S4)[28], were treated with compound **2** ([**2**] = 50 μM, 4 h, pH = 7.4, 37 °C). Following compound incubation, the cells were lysed, and target engagement was determined *via* a label-free chemoproteomics workflow employing a hyper-reactive iodoacetamide-desthiobiotin competitor.[29] This enabled quantification of the extent of covalent modification of M^{Pro} and allowed for identification of the site of binding. Compound **2** was observed to engage the catalytic cysteine of M^{Pro} (Cys145) in live cells with 77 % occupancy ($\log_2$ competition ratio = 2.1, Figure 1H). The chemoproteomic workflow also enabled the quantification of off-target cysteine engagement against 6,827 cysteine residues within 3,459 proteins of the A549 proteome. In total, 14 off-target cysteines had a competition ratio greater than four when compared to DMSO (> 75 % occupancy), and 11 were more strongly competed than M^{Pro} Cys145. Four of the 14 cysteines were active site cysteines, of which one was the active site of a thiol protease (DESI2 Cys108, Figure S5).

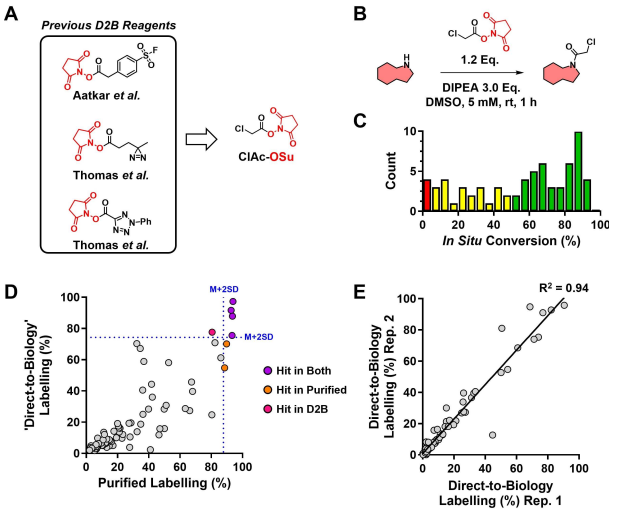

Figure 2. Development of a 'direct-to-biology' approach for synthesising and screening chloroacetamide reactive fragments. (A) Previous literature surrounding the application of N-hydroxysuccinimide activated esters for 'direct-to-biology' screening of reactive fragments.[18] (B) The synthetic conditions employed in the picomolar-scale synthesis of chloroacetamide reactive fragments. (C) The calculated in situ conversion for a pilot library of 69 chloroacetamides synthesised via the high-throughput conditions. In situ conversion was calculated as the UV TIC area-under-curve of the product-containing peak detected by small molecule LC-MS. The product containing peak was selected on the observation of the expected $[M+H]^+$ m/z ion. (D) A comparison of the M^{Pro} labelling by a library of chloroacetamide fragments screened as purified and crude analogues. Chloroacetamides were screened at an (assumed) concentration of 50 μM against M^{Pro} (0.5 μM) for 16 hours at 4 °C before determination of the extent of labelling by IP-LC/MS. (E) A comparison of the extent of M^{Pro} labelling for two experimental replicates of the high-throughput synthesis and screening of crude chloroacetamides. Reproducibility was determined by the coefficient of deviation (R^2) of a linear regression fit.

Development of a High-Throughput Synthesis, 'Direct-to-Biology' Screening Approach for Reactive Fragments Targeting SARS-CoV-2 M^{Pro}

To optimise the hits against SARS-CoV-2 M^{Pro} using the envisaged D2B approach, appropriate synthetic conditions for the high-throughput synthesis of chloroacetamide RFs were required. Previous examples of reactive fragment D2B workflows employed a reactive-group building block functionalised with an *N*-hydroxysuccinimide activated ester.[18] Thus, it was hypothesised that the *N*-hydroxysuccinimide ester of chloroacetic acid (ClAc-OSu) would enable the preparation of chloroacetamide fragments (Figure 2A). The reagent was readily synthesised on a multi-gram scale, and in initial tests resulted in near-complete conversion of a model amine to the chloroacetamide product at a 200 pmol scale within a 384-well plate (Figure S6). Encouraged by this result, the parallel synthesis of a library of 69 chloroacetamide reactive fragments was performed (Figure 2B). Analysis of the reaction performance employing small-molecule LC/MS and automated reaction analysis scripting highlighted good reaction performance (Figure 2C).[30] More than half of the intended chloroacetamides were present as the major component of the reaction mixture (in situ conversion > 50 %, 43 compounds), while just four chloroacetamides were not detected as reaction products. For further details regarding the chemistry optimisation campaign, please refer to section S1.1 in the Supporting Information.

Following the identification of suitable high-throughput chemistry conditions, the accuracy of D2B screening was evaluated. The synthesised library of 69 chloroacetamides was chosen to be a sub-set of the 219-member library initially screened against M^{Pro} to enable comparison of screening results obtained from crude and purified libraries. Consequently, both the library of crude chloroacetamides and their purified counterparts were incubated with M^{Pro} at an (assumed) concentration of 50 μM for 16 hours at 4 °C, and the extent of covalent labelling was assessed *via* IP-LC/MS. The screen was performed at a higher concentration to ensure a greater proportion of active fragments for comparison. The resulting labelling was in good agreement with that measured using purified compounds (Figure 2D). A hit-calling threshold of covalent engagment that surpassed the mean plus two standard deviations across each respective library was applied to identify false positives and negatives. Of the six confirmed hits identified by screening purified fragments, four were also identified as hits in the D2B

screen. Screening performance of the D2B library was not improved by increasing the equivalents of ClAc-OSu employed in the synthesis of chloroacetamides (Figure S7). To assess the reproducibility of the protocol, the high-throughput synthesis and D2B screening of the 69-membered library was evaluated in two experimental replicates, affording excellent reproducibility of M^{Pro} labelling ($R^2 = 0.94$, Figure 2E).

'Direct-to-Biology' Screening Enabled the Rapid Optimisation of Reactive Fragment Inhibitors of M^{Pro}

With a validated method for D2B screening of chloroacetamide libraries obtained, we sought to employ this approach for the optimisation of fragment **2**. To probe the SAR landscape, a 193-member library of amine analogues was designed by selecting amines similar to **2** from the GSK library using the small-world algorithm.[31] This selection primarily consisted of three common substructures: 2-aryl morpholines (65), 2-heteroaryl morpholines (48), 3-aryl pyrrolidines (48) and 32 structures with no common scaffold (Figure 3A). Synthesis of the analogue library afforded 77 % of the intended chloroacetamide products as the major reaction component, with just nine instances where no chloroacetamide was detected, corresponding to a 4 % failure rate (Figure 3B).

The library was screened against M^{Pro}, with the extent of covalent modification determined *via* IP-LC/MS. Anticipating an improvement in the overall activity of the library, the compounds were screened at an assumed concentration of 5 μM for just one hour at 4 °C (vs 16 h previously). A formic acid quench (0.4 %) was employed to halt further labelling after the one hour incubation.[7b] Despite the shorter incubation time, 14 compounds were identified that exceeded 75 % labelling (Figure 3C). In addition to identifying highly active ligands for M^{Pro}, the analogue library provided an opportunity to develop an understanding of the SAR. A hierarchical clustering of the library was performed using extended connectivity fingerprints (ECFP4)[32], compounds were then annotated with the corresponding percentage labelling. Only compounds that were formed as the major component were included in this analysis to reduce the risk of misinterpreting false negatives. The resulting visualisation facilitated identification of regions of activity and inactivity, as well as the effects of individual point-changes (Figure 3D, Figure S8).

We next sought to determine the inhibitory potencies of the 14 newly identified RF hits. Initially the crude reaction products were screened directly, following validation of the FRET inhibitory assay for D2B screening (Figure S9). All 14 hits resulted in M^{Pro} inhibition following a one hour incubation, with pIC_{50} (1 h) values ranging from 5.1–7.4 (Figure S10). Compounds **7**, **8** and **9** exhibited the strongest inhibition of M^{Pro}, with a 10-fold or greater improvement in potency compared to fragment **2** (Figure 3E). The activity of compound **7** (pIC_{50} (1 h) >7.4) was remarkable given it maintained fragment-like physicochemical properties (HBA = 1, HBD = 0, cLogP = 2.9, MW = 305, R.B. = 3, tPSA = 20.3).

To validate the observed inhibitory activity of **7**, it was resynthesised and screened as a purified compound. The enantiomer of **7** (**7b**, 1*S*,5*R*) was also synthesised to determine any enantioselectivity. The original enantiomer (**7**(**a**), 1*R*,5*S*) maintained strong potency following a one-hour incubation (pIC_{50} (1 h) >7.4) whilst the opposite enantiomer (**7b**) demonstrated reduced potency (pIC_{50} (1 h) = 6.9, Figure S11). The second-order rate constant of covalent inhibition (k_{inact}/K_I) for each enantiomer was indeterminable, due to the rapid onset of inhibition. Instead, the time-dependence of the IC_{50} was measured.[33] Both enantiomers exhibited a time-dependent change in IC_{50} consistent with that of a two-step irreversible mechanism of action, with **7a** exhibiting a faster onset of inhibition reaching an IC_{50} at the limit of the assay (40 nM) after 46 min (c.f. IC_{50} of **7b** = 170 nM at the equivalent timepoint, Figure 3F). This represents a >32-fold improvement in potency from the initial hit **2** to **7a**, following a single round of D2B screening. The intrinsic reactivity of **7** was found to have increased ~3-fold compared to compound **2**, according to the GSH reactivity assay (Figure S12). Despite the increased reactivity, the >32-fold potency improvement indicates an improvement in the reversible affinity of the fragment.

Engagement of M^{Pro} Cys145 by compound **7a** in live cells was confirmed by chemoproteomics. When compared to fragment **2**, labelling of M^{Pro} was improved to 80 % (log_2 competition ratio = 2.4) and the number of off-targets was halved from fourteen to seven (Figure 3G). Of the off-targets identified, none were thiol proteases and no active site cysteines were significantly engaged (Figure S5). The activity of compound **7a** was also measured against an emerging mutant form of M^{Pro} which confers resistance to nirmatrelvir.[8] Sequence analysis highlights that mutation of Ser144 results in the loss of an oxyanion hole within the active site, which is commonly engaged by M^{Pro} inhibitors.[34] Following treatment of A549 cells expressing the S144A mutant M^{Pro} with compound **7a** under analagous conditions to the wild-type screening ([2] = 50 μM, 4 hours), chemoproteomics confirmed engagement of mutant M^{Pro} with occupancy of 78 %, comparable to that of the wild-type (80 %, Figure 3H).

Progression of a Potent Inhibitor of M^{Pro} through Electrophilicity Tuning and a Non-Covalent 'Switch'

Having optimised the initial chloroacetamide fragment hit **2** to potent inhibitor **7** *via* D2B screening, we next explored opportunities to: i) lower the reactivity of the electrophile to reduce off target liabilities while maintaining on target activity; ii) remove the electrophile to afford non covalent inhibitors.

Three analogues of compound **7** were designed and synthesised to incorporate a 1-chloro-1-fluoroacetamide electrophile (**10**), 1-fluoroacetamide electrophile (**11**),[35] and a non-electrophilic, acetamide analogue (**12**) (Figure 4A). The intrinsic reactivities of compounds **10** and **11** were

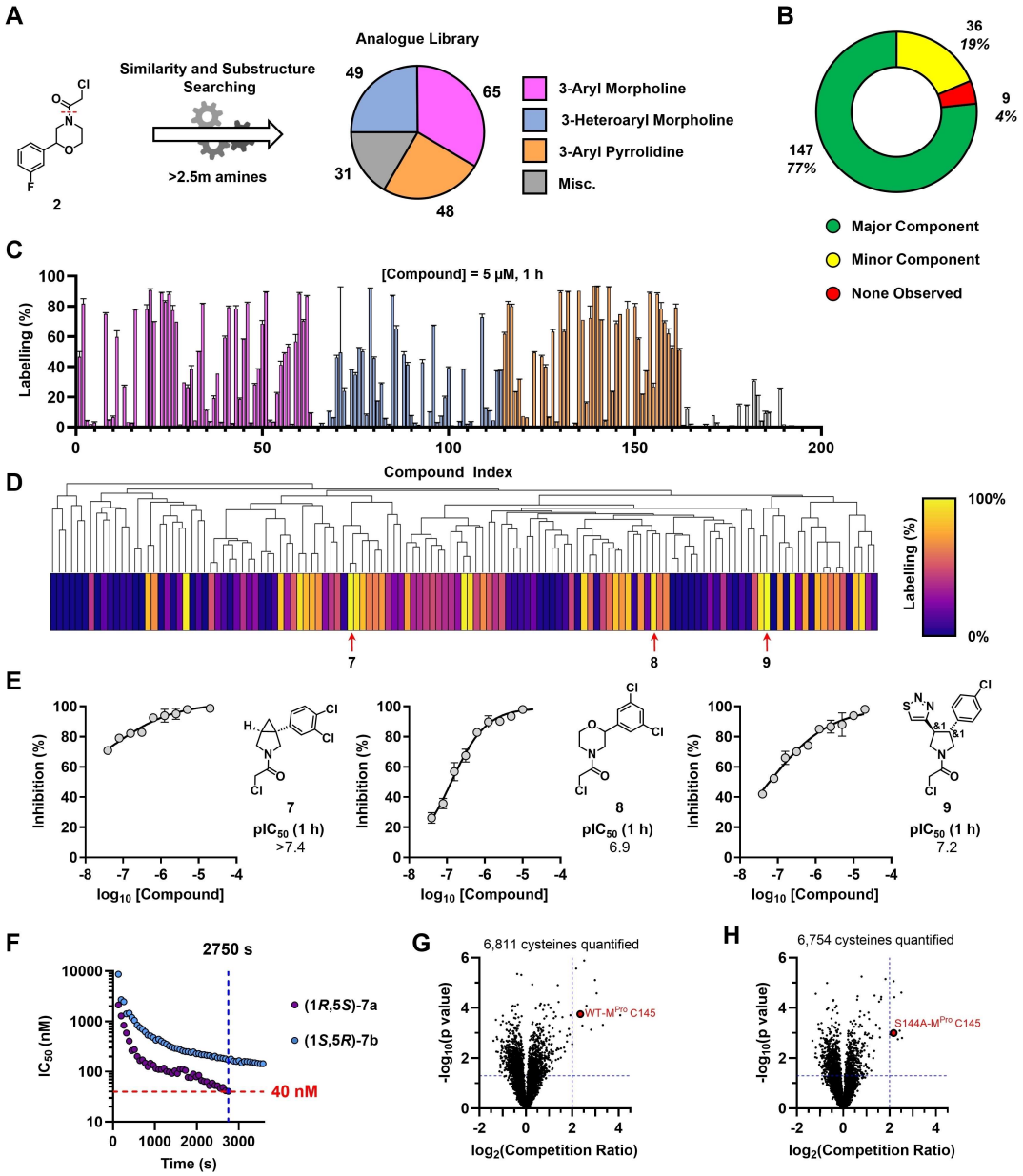

Figure 3. Application of the 'direct-to-biology' platform for the optimisation of initial fragment hit **2**. (A) A blended small-world and substructural small-world approach was used in the selection of analogues to the hit fragment **2**. This resulted in the selection of 193 amines which were binned into four categories, based upon common substructures. (B) The observed reaction performance for the analogue library, binned according to the calculated in situ conversion by small molecule LC-MS. (C) The extent of covalent labelling for the 193-membered analogue library as determined by IP-LC/MS. Compounds were screened at an assumed concentration of 5 µM for one hour, followed by a formic acid quench (0.4% *v*/*v*). Data shown is the mean across two technical replicates, with error bars showing the standard deviation. Data points have been coloured according to the compound's substructure class. (D) A hierarchical clustering of the analogue library based upon the ECFP4 fingerprints of each structure. Only compounds formed as the major component of the reaction were considered. The extent of M^{Pro} labelling for each compound is also shown, allowing for the identification of areas of active and inactive structures. The three top hits identified from the screen are also highlighted. (E) The concentration dependent inhibition of M^{Pro} activity following a one-hour incubation of the crude D2B reaction mixture for chloroacetamides **7**, **8** and **9**. Data shown is the mean across two biological replicates, with error bars showing the standard deviation. (F) The time dependent M^{Pro} IC_{50} of the two enantiomers of fragment **7**. The sensitivity of the assay was met after 2750 seconds for the (1R, 5S) enantiomer. (G, H) A volcano plot denoting the mean log_2-transformed competition ratio (CR) and associated -log_{10}-transformed *p*-value for each detected cysteine across four technical replicates of compound **7** and DMSO treatments in A549 cells transduced to express wild-type M^{Pro} (G) and S144A mutant M^{Pro} (H). Calculated *p*-values were derived from the Welch's unpaired t-test. A significance threshold of $p < 0.05$ and a CR > 4 was selected. The detected peptide corresponding to M^{Pro} Cys145 has been highlighted.

assessed: **11** was found to be unreactive with glutathione ($t_{1/2} > 24$ h), while a $t_{1/2}$ could not be determined for compound **10** due to poor solubility. Electrophilic compounds **10** and **11** were screened against M^{Pro} by IP-LC/MS to assess

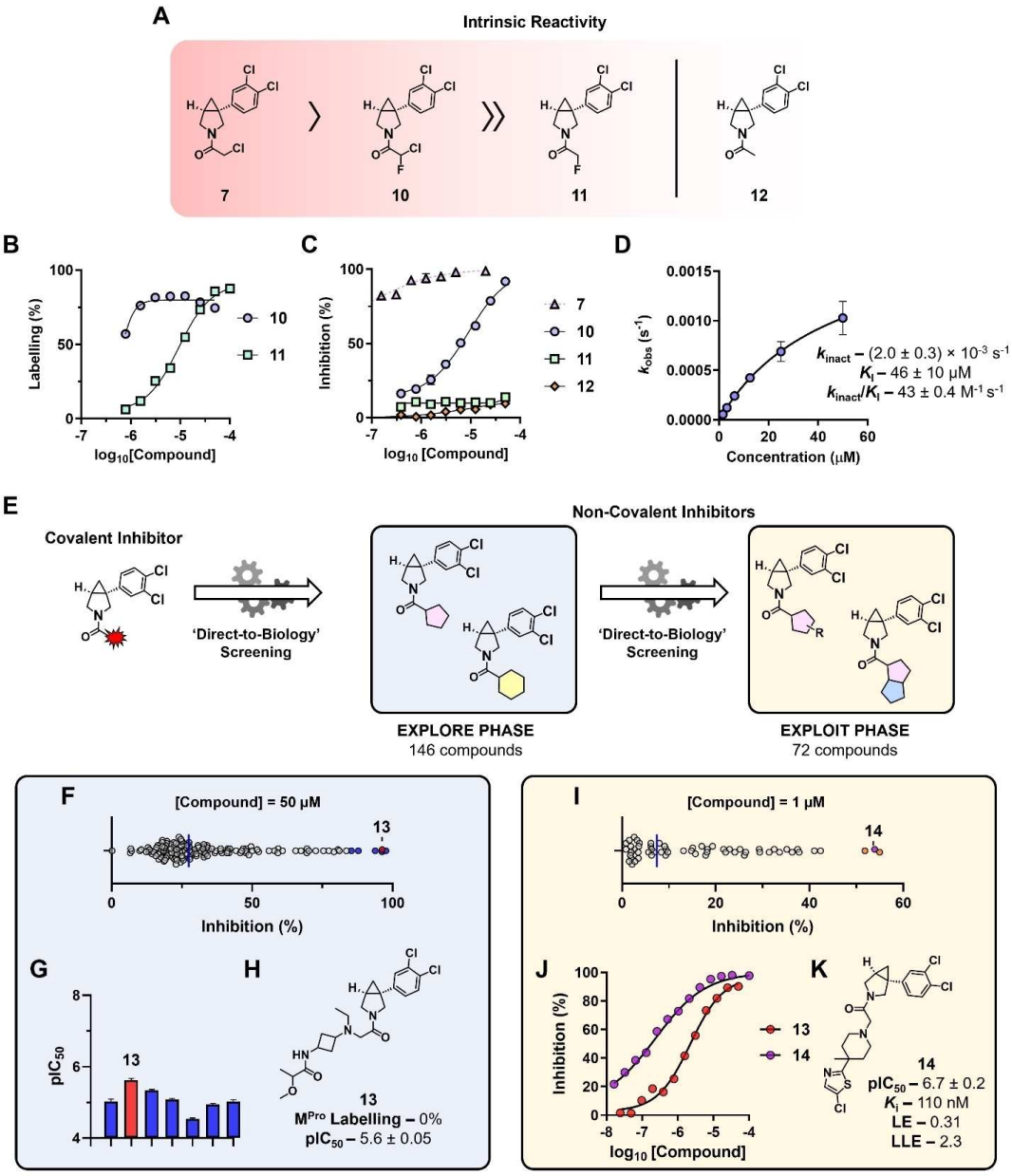

Figure 4. (A) The design of three analogues of **7** wherein the reactivity of the electrophilic position was reduced, or the electrophile was removed. (B) The concentration-dependence of M^{Pro} labelling following a 24 hour incubation of **10** and **11**. A pIC_{50} for each compound was calculated using a four-parameter variable slope fit. (C) The concentration-dependent inhibition of M^{Pro} activity following a one-hour incubation with compounds **10**, **11** and **12**. Data shown is the mean and standard deviation across two biological replicates. For comparison, the previously determined pIC_{50} curve for **7** is shown. (D) The concentration-dependence of the observed rate of inhibition of M^{Pro} by compound **10**. A non-linear relationship was observed, which allowed for determination of the kinetic parameters K_I and k_{inact} by a Michaelis-Menten fit. Data shown is the mean and standard deviation across two biological replicates. (E) Employment of high-throughput synthesis and 'direct-to-biology' screening to progress compound **7** into a non-covalent inhibitor series. Two distinct stages of compound optimisation were performed – an initial explore phase wherein non-covalent inhibitors were discovered, and an exploit phase wherein the potency of these compounds was improved. (F) The measured M^{Pro} inhibition when the explore library was screened. Compounds were pre-incubated with M^{Pro} (10 nM) at an assumed concentration of 50 μM for 15 minutes, prior to the addition of the FRET substrate. Inhibition was calculated following a one hour incubation. Hits, identified as blue or red dots, were those which surpassed the 95th percentile of M^{Pro} inhibition. The mean inhibition across the library is shown as a blue bar. (G) Calculated pIC_{50} values for the seven identified hits. pIC_{50} values were calculated from a single technical replicate, data shown is the calculated pIC_{50} and corresponding error of fit. (H) The structure and activity of the most potent non-covalent inhibitor of M^{Pro} identified in the explore phase. The compound was counter-screened *via* IP-LC/MS which confirmed no covalent adduct formation. (I) The measured M^{Pro} inhibition when the exploit library was screened. Compounds were screened under analogous conditions to (F) at a lower assumed concentration. Hits, identified as orange or purple dots, were compounds that exhibited greater than 50% inhibition of M^{Pro}. The mean inhibition across the library is shown as a blue bar. (J) The concentration-dependent inhibition of compounds **13** and **14**, identified as the most potent inhibitors of M^{Pro} from the explore and exploit phase respectively. (K) The structure and reversible affinity and efficiency of compound **14**, which resulted in the greatest inhibitory potency of M^{Pro} of the non-covalent analogues examined.

covalent engagement (0.8–200 μM, 24 h, 4 °C). Despite the reduced reactivity of the electrophiles, concentration-dependent labelling of M^{Pro} was observed for both compounds, with calculated pIC_{50} values of >6.2 and 5.0 ± 0.05 respectively (Figure 4B). Encouraged by the confirmation of covalent labelling, subsequently, M^{Pro} inhibitory potencies of **10** and **11** were determined by FRET following a one hour incubation (Figure 4C). Compound **10** inhibited M^{Pro} with a pIC_{50} (1 h) $= 5.1 \pm 0.06$, while compound **11** was inactive after this reduced incubation time (1 h vs 24 h for IP-LC/MS). Compound **10** exhibited a non-linear relationship between concentration and k_{obs} across the concentrations evaluated, enabling calculation of the kinetic parameters of inhibition: $k_{inact} = (2.0 \pm 0.03) \times 10^{-3}\ s^{-1}$ and $K_I = 46 \pm 10$ μM ($k_{inact}/K_I = 43 \pm 0.4\ M^{-1}\ s^{-1}$, Figure 4D). While these compounds exhibit a reduction in potency relative to **7**, likely resulting from a reduction in k_{inact}, the confirmation of covalent labelling with these less reactive electrophiles makes them promising candidates for optimisation towards more developable M^{Pro} inhibitors. To our knowledge, compound **11** represents the first example of a reactive fragment ligand for a protein employing a fluoroacetamide.

With a view to developing non-covalent inhibitors of M^{Pro}, compound **12** was screened in the FRET assay. While an IC_{50} value was not measurable due to low activity (maximum inhibition $= 9.5 \pm 0.5$ % at 50 μM), we hypothesised that active non-covalent analogues of compound **7** might be discovered by substituting the chloroacetamide electrophile with alternative amides that may facilitate molecular recognition of the M^{Pro} binding site. We envisaged D2B screening could enable rapid optimisation of this group within two rounds, firstly sampling chemical space ("explore" phase) and subsequently expanding on emerging hits ("exploit" phase, Figure 4E).[36] A diverse set of 146 carboxylic acids were selected using the small-world algorithm[31] from the GSK compound collection (Figure S13), and linked to the amine precursor of compound **7** using HATU-mediated amide coupling in 384-well plates (Figure S14). The library was screened against M^{Pro} using the FRET inhibitory assay (assumed compound concentration: 50 μM, 15 minutes pre-incubation). Control experiments confirmed that the reagents and by-products of the synthesis had minimal impact on the activity of M^{Pro} (Figure S15). Seven compounds were identified which surpassed the 95th percentile of M^{Pro} inhibition (Figure 4F) and counter-screening with IP-LC/MS confirmed no covalent adducts were formed (Figure S16). Half-maximal inhibitory potency against M^{Pro} was determined for each hit compound, which identified compound **13** as the most potent ($pIC_{50} = 5.6 \pm 0.07$, Figure 4G), with a potency similar to RF **2** after one hour, despite the absence of an electrophile (Figure 4H).

The exploit library, consisting of 72 carboxylic acids, was designed around compound **13**. Compounds were screened against M^{Pro} at a lowered assumed concentration of 1 μM, maintaining the 15 minute pre-incubation (Figure 4I). Three compounds were identified with >50 % inhibition of M^{Pro}, which upon further examination demonstrated concentration-dependent inhibition and an improved potency over compound **13**, with pIC_{50} values between 6.2–6.7 (Figure S17). Compound **14** was the most potent inhibitor identified ($pIC_{50} = 6.7 \pm 0.2$) (Figure 4J). Using the Cheng-Prusoff equation, the reversible inhibitory affinity (K_I) of compound was determined to be 110 nM, representing a >400-fold improvement in reversible binding affinity over compound **10** (c.f. $K_I = 46$ μM).[37] Further characterisation of compound **14** highlighted good ligand efficiency (LE = 0.31 vs 0.32 for compound **10**) and an acceptable lipophilic ligand efficiency (cLogD (pH 7.4) = 4.4, LLE = 2.3), suggesting the suitability of this compound for further lead development.[11,38]

Conclusion

The continued development of novel therapeutics is essential to counteract emerging SARS-CoV-2 mutants and maintain preparedness for future coronaviruses. The main protease is an established drug target, due to its essential role in the viral lifecycle and conservation within the *Coronaviridae* family. The activity of coronavirus' M^{Pro} is dependent upon a catalytic cysteine, therefore covalent modification of this residue is an attractive approach to inhibitor discovery. To enable the rapid development of irreversible M^{Pro} inhibitors in response to emerging coronaviruses, high-throughput methods to synthesise and profile cysteine-targeting compounds are required. We report the development of a 'direct-to-biology' platform for the identification and optimisation of chloroacetamide reactive fragments, applied towards the discovery of potent SARS-CoV-2 M^{Pro} inhibitors.

'Direct-to-biology' screening enabled rapid discovery of a highly potent inhibitor (**7**) that irreversibly and potently inhibits M^{Pro} within one hour. Compound **7** was found to covalently modify the catalytic cysteine (Cys145) and demonstrated strong cellular engagement of wild-type M^{Pro}. We also demonstrated the ability of this fragment to engage the catalytic cysteine of the S144A mutant of M^{Pro}, which represents an emerging class of clinically relevant M^{Pro} mutations that can escape inhibition by nirmatrelvir. During the discovery of compound **7**, the insights obtained from D2B screening enabled the rapid exploration and exploitation of structure-activity relationships, providing opportunity for an expedited and flexible optimisation strategy. As this approach matures, we envisage D2B screening would be amenable to machine learning techniques to provide quantitative and predictive insights.[39]

Chloroacetamides are often considered unsuitable for applications *in vivo* due to concerns with the high intrinsic electrophilicity and the potential for off-target interactions. We therefore developed a strategy to tune the reactivity by incorporation of electrophiles with reduced reactivity but conserved reaction geometries. The resulting compounds maintained activity with M^{Pro}, but had significantly reduced electrophilicity, thus offering useful starting points for the development of next generation M^{Pro} inhibitors. The partnership of D2B fragment optimisation with tunable warheads offers a useful strategy to facilitate identification of

hits, followed by optimisation to more potent and selective inhibitors. We note that irreversible inhibitors of M^{Pro} have been reported with very high second-order rate constants, highlighting that further optimisation of potency is achievable.[40] Finally, the D2B platform enabled evolution of the covalent inhibitors into a non-covalent series: within two D2B cycles, a potent and efficient non-covalent inhibitor (**14**) was discovered. This is an under-reported drug discovery strategy that can leverage the advantages of irreversible mechanisms of action in early-stage hit discovery while providing flexibility for optimisation towards either covalent or non-covalent inhibitors.

Acknowledgements

H. W. is grateful to GSK for a studentship *via* the GSK/University of Strathclyde Centre for Doctoral Training in Synthetic and Medicinal Chemistry. We thank Stephen Besley and Omar Rahman for support with the acquisition of LC-MS data. We thank Randy Bledsoe for the expression and purification of SARS-CoV-2 M^{Pro}. We thank Peter Pogany for support in the selection of compounds. This work was supported by the Francis Crick Institute, which receives its core funding from Cancer Research UK (CC2075), the UK Medical Research Council (CC2075), and the Wellcome Trust (CC2075), and by the Engineering and Physical Sciences Research Council, EP/V038028/1.

Data Availability

The mass spectrometry proteomics data have been deposited to the ProteomeXchange Consortium via the PRIDE partner repository with the dataset identifier PXD056098.

Conflict of Interest

The authors declare no conflict of interest.

Keywords: Direct-to-Biology · Inhibitors · Medicinal Chemistry · Reactive Fragment · SARS-CoV-2 M^{Pro}

[1] a) D. R. Owen, C. M. N. Allerton, A. S. Anderson, L. Aschenbrenner, M. Avery, S. Berritt, B. Boras, R. D. Cardin, A. Carlo, K. J. Coffman, A. Dantonio, L. Di, H. Eng, R. Ferre, K. S. Gajiwala, S. A. Gibson, S. E. Greasley, B. L. Hurst, E. P. Kadar, A. S. Kalgutkar, J. C. Lee, J. Lee, W. Liu, S. W. Mason, S. Noell, J. J. Novak, R. S. Obach, K. Ogilvie, N. C. Patel, M. Pettersson, D. K. Rai, M. R. Reese, M. F. Sammons, J. G. Sathish, R. S. P. Singh, C. M. Steppan, A. E. Stewart, J. B. Tuttle, L. Updyke, P. R. Verhoest, L. Wei, Q. Yang, Y. Zhu, *Science* **2021**, *374*, 1586–1593; b) F. Krammer, *Nature* **2020**, *586*, 516–527; c) C. M. N. Allerton, J. T. Arcari, L. M. Aschenbrenner, M. Avery, B. M. Bechle, M. A. Behzadi, B. Boras, L. M. Buzon, R. D. Cardin, N. R. Catlin, A. A. Carlo, K. J. Coffman, A. Dantonio, L. Di, H. Eng, K. A. Farley, R. A. Ferre, S. S. Gernhardt, S. A. Gibson, S. E. Greasley, S. R. Greenfield, B. L. Hurst, A. S. Kalgutkar, E. Kimoto, L. F. Lanyon, G. H. Lovett, Y. Lian, W. Liu, L. A. Martínez Alsina, S. Noell, R. S. Obach, D. R. Owen, N. C. Patel, D. K. Rai, M. R. Reese, H. A. Rothan, S. Sakata, M. F. Sammons, J. G. Sathish, R. Sharma, C. M. Steppan, J. B. Tuttle, P. R. Verhoest, L. Wei, Q. Yang, I. Yurgelonis, Y. Zhu, *Journal of Medicinal Chemistry* **2024**.

[2] B. Tan, X. Zhang, A. Ansari, P. Jadhav, H. Tan, K. Li, A. Chopra, A. Ford, X. Chi, F. X. Ruiz, E. Arnold, X. Deng, J. Wang, *Science* **2024**, *383*, 1434–1440.

[3] W. Yan, Y. Zheng, X. Zeng, B. He, W. Cheng, *Signal Transduction and Targeted Therapy* **2022**, *7*, 26.

[4] A. Zumla, J. F. W. Chan, E. I. Azhar, D. S. C. Hui, K.-Y. Yuen, *Nature Reviews Drug Discovery* **2016**, *15*, 327–347.

[5] Y. R. Alugubelli, J. Xiao, K. Khatua, S. Kumar, L. Sun, Y. Ma, X. R. Ma, V. R. Vulupala, S. Atla, L. R. Blankenship, D. Coleman, X. Xie, B. W. Neuman, W. R. Liu, S. Xu, *Journal of Medicinal Chemistry* **2024**, *67*, 6495–6507.

[6] a) J. Johansen-Leete, S. Ullrich, S. E. Fry, R. Frkic, M. J. Bedding, A. Aggarwal, A. S. Ashhurst, K. B. Ekanayake, M. C. Mahawaththa, V. M. Sasi, S. Luedtke, D. J. Ford, A. J. O'Donoghue, T. Passioura, M. Larance, G. Otting, S. Turville, C. J. Jackson, C. Nitsche, R. J. Payne, *Chem Sci* **2022**, *13*, 3826–3836; b) R. Jimmidi, S. Chamakuri, S. Lu, M. N. Ucisik, P.-J. Chen, K. M. Bohren, S. A. Moghadasi, L. Versteeg, C. Nnabuife, J.-Y. Li, X. Qin, Y.-C. Chen, J. C. Faver, P. Nyshadham, K. L. Sharma, B. Sankaran, A. Judge, Z. Yu, F. Li, J. Pollet, R. S. Harris, M. M. Matzuk, T. Palzkill, D. W. Young, *Communications Chemistry* **2023**, *6*, 164.

[7] a) P. Moon, C. M. Zammit, Q. Shao, D. Dovala, L. Boike, N. J. Henning, M. Knapp, J. N. Spradlin, C. C. Ward, H. Wolleb, D. Fuller, G. Blake, J. P. Murphy, F. Wang, Y. Lu, S. A. Moquin, L. Tandeske, M. J. Hesse, J. M. McKenna, J. A. Tallarico, M. Schirle, F. D. Toste, D. K. Nomura, *ChemBioChem* **2023**, *24*, e202300116; b) A. Douangamath, D. Fearon, P. Gehrtz, T. Krojer, P. Lukacik, C. D. Owen, E. Resnick, C. Strain-Damerell, A. Aimon, P. Ábrányi-Balogh, J. Brandão-Neto, A. Carbery, G. Davison, A. Dias, T. D. Downes, L. Dunnett, M. Fairhead, J. D. Firth, S. P. Jones, A. Keeley, G. M. Keserü, H. F. Klein, M. P. Martin, M. E. M. Noble, P. O'Brien, A. Powell, R. N. Reddi, R. Skyner, M. Snee, M. J. Waring, C. Wild, N. London, F. von Delft, M. A. Walsh, *Nature Communications* **2020**, *11*, 5047.

[8] Y. Hu, E. M. Lewandowski, H. Tan, X. Zhang, R. T. Morgan, X. Zhang, L. M. C. Jacobs, S. G. Butler, M. V. Gongora, J. Choy, X. Deng, Y. Chen, J. Wang, *ACS Cent. Sci.* **2023**, *9*, 1658–1669.

[9] J. Heskin, S. J. C. Pallett, N. Mughal, G. W. Davies, L. S. P. Moore, M. Rayment, R. Jones, *Lancet* **2022**, *399*, 21–22.

[10] L. Boike, N. J. Henning, D. K. Nomura, *Nat. Rev. Drug Discov.* **2022**, *21*, 881–898.

[11] A. L. Hopkins, C. R. Groom, A. Alex, *Drug Discov. Today* **2004**, *9*, 430–431.

[12] a) Y. Shin, J. W. Jeong, R. P. Wurz, P. Achanta, T. Arvedson, M. D. Bartberger, I. D. G. Campuzano, R. Fucini, S. K. Hansen, J. Ingersoll, J. S. Iwig, J. R. Lipford, V. Ma, D. J. Kopecky, J. McCarter, T. San Miguel, C. Mohr, S. Sabet, A. Y. Saiki, A. Sawayama, S. Sethofer, C. M. Tegley, L. P. Volak, K. Yang, B. A. Lanman, D. A. Erlanson, V. J. Cee, *ACS Med. Chem. Lett.* **2019**, *10*, 1302–1308; b) L. Boike, A. G. Cioffi, F. C. Majewski, J. Co, N. J. Henning, M. D. Jones, G. Liu, J. M. McKenna, J. A. Tallarico, M. Schirle, D. K. Nomura, *Cell Chem. Biol.* **2021**, *28*, 4–13.e17; c) X. Xie, T. Yu, X. Li, N. Zhang, L. J. Foster, C. Peng, W. Huang, G. He, *Signal Transduct. Target. Ther.* **2023**, *8*, 335.

[13] a) H. Johansson, Y.-C. I. Tsai, K. Fantom, C.-W. Chung, S. Kümper, L. Martino, D. A. Thomas, H. C. Eberl, M. Muelbaier, D. House, K. Rittinger, *J. Am. Chem. Soc.* **2019**, *141*, 2703–

2712; b) G. B. Craven, D. P. Affron, C. E. Allen, S. Matthies, J. G. Greener, R. M. L. Morgan, E. W. Tate, A. Armstrong, D. J. Mann, *Angew. Chem. Int. Ed.* **2018**, *57*, 5257–5261; c) M. Jamshidiha, T. Lanyon-Hogg, C. L. Sutherell, G. B. Craven, M. Tersa, E. De Vita, D. Brustur, I. Pérez-Dorado, S. Hassan, R. Petracca, R. M. Morgan, M. Sanz-Hernández, J. C. Norman, A. Armstrong, D. J. Mann, E. Cota, E. W. Tate, *RSC Med. Chem.* **2022**, *13*, 150–155.

[14] S. Chow, S. Liver, A. Nelson, *Nat. Rev. Chem.* **2018**, *2*, 174–183.

[15] a) A. Brik, J. Muldoon, Y.-C. Lin, J. H. Elder, D. S. Goodsell, A. J. Olson, V. V. Fokin, K. B. Sharpless, C.-H. Wong, *ChemBioChem* **2003**, *4*, 1246–1248; b) B. Mahjour, R. Zhang, Y. Shen, A. McGrath, R. Zhao, O. G. Mohamed, Y. Lin, Z. Zhang, J. L. Douthwaite, A. Tripathi, T. Cernak, *Nat. Commun.* **2023**, *14*, 3924.

[16] a) R. Stevens, E. Bendito-Moll, D. J. Battersby, A. H. Miah, N. Wellaway, R. P. Law, P. Stacey, D. Klimaszewska, J. M. Macina, G. A. Burley, J. D. Harling, *J. Med. Chem.* **2023**, *66*, 15437–15452; b) L. Guo, Y. Zhou, X. Nie, Z. Zhang, Z. Zhang, C. Li, T. Wang, W. Tang, *Eur. J. Med. Chem.* **2022**, *236*, 114317.

[17] a) A. Ng, F. Offensperger, J. A. Cisneros, N. S. Scholes, M. Malik, L. Villanti, A. Rukavina, E. Ferrada, J. T. Hannich, A. Koren, S. Kubicek, G. Superti-Furga, G. E. Winter, *ACS Chem. Biol.* **2023**, *18*, 2464–2473; b) J. Li, C. Li, Z. Zhang, Z. Zhang, Z. Wu, J. Liao, Z. Wang, M. McReynolds, H. Xie, L. Guo, Q. Fan, J. Peng, W. Tang, *Eur. J. Med. Chem.* **2023**, *258*, 115567; c) Z. Wang, S. Shaabani, X. Gao, Y. L. D. Ng, V. Sapozhnikova, P. Mertins, J. Krönke, A. Dömling, *Nat. Commun.* **2023**, *14*, 8437.

[18] a) R. P. Thomas, E. K. Grant, E. R. Dickinson, F. Zappacosta, L. J. Edwards, M. M. Hann, D. House, N. C. O. Tomkinson, J. T. Bush, *RSC Med. Chem.* **2023**, *14*, 671–679; b) A. Aatkar, A. Vuorinen, O. E. Longfield, K. Gilbert, R. Peltier-Heap, C. D. Wagner, F. Zappacosta, K. Rittinger, C.-w. Chung, D. House, N. C. O. Tomkinson, J. T. Bush, *ACS Chem. Biol.* **2023**, *18*, 1926–1937; c) R. P. Thomas, R. E. Heap, F. Zappacosta, E. K. Grant, P. Pogány, S. Besley, D. J. Fallon, M. M. Hann, D. House, N. C. O. Tomkinson, J. T. Bush, *Chem. Sci.* **2021**, *12*, 12098–12106.

[19] M. Congreve, R. Carr, C. Murray, H. Jhoti, *Drug Discov. Today* **2003**, *8*, 876–877.

[20] D. J. Fallon, A. Phillipou, C. J. Schofield, D. House, N. C. O. Tomkinson, J. T. Bush, *Biochem. J.* **2023**, *480*, 1183–1197.

[21] E. K. Grant, D. J. Fallon, M. M. Hann, K. G. M. Fantom, C. Quinn, F. Zappacosta, R. S. Annan, C.-w. Chung, P. Bamborough, D. P. Dixon, P. Stacey, D. House, V. K. Patel, N. C. O. Tomkinson, J. T. Bush, *Angew. Chem. Int. Ed.* **2020**, *59*, 21096–21105.

[22] L. S. Barton, J. F. Callahan, J. Cantizani, N. O. Concha, I. Cotillo Torrejon, N. C. Goodwin, A. Joshi-Pangu, T. J. Kiesow, J. J. McAtee, M. Mellinger, C. J. Nixon, L. Padrón-Barthe, J. R. Patterson, N. D. Pearson, J. J. Pouliot, A. R. Rendina, A. Buitrago Santanilla, J. L. Schneck, O. Sanz, R. K. Thalji, P. Ward, S. P. Williams, B. W. King, *Bioorg. Med. Chem.* **2024**, *100*, 117618.

[23] J. M. Strelow, *SLAS Discov.* **2017**, *22*, 3–20.

[24] M. Gehringer, S. A. Laufer, *J. Med. Chem.* **2019**, *62*, 5673–5724.

[25] N. Shindo, A. Ojida, *Bioorg. Med. Chem.* **2021**, *47*, 116386.

[26] S. Butterworth, D. A. E. Cross, M. R. V. Finlay, R. A. Ward, M. J. Waring, *Medchemcomm* **2017**, *8*, 820–822.

[27] E. Resnick, A. Bradley, J. Gan, A. Douangamath, T. Krojer, R. Sethi, P. P. Geurink, A. Aimon, G. Amitai, D. Bellini, J. Bennett, M. Fairhead, O. Fedorov, R. Gabizon, J. Gan, J. Guo, A. Plotnikov, N. Reznik, G. F. Ruda, L. Díaz-Sáez, V. M. Straub, T. Szommer, S. Velupillai, D. Zaidman, Y. Zhang, A. R. Coker, C. G. Dowson, H. M. Barr, C. Wang, K. V. M. Huber, P. E. Brennan, H. Ovaa, F. von Delft, N. London, *J. Am. Chem. Soc.* **2019**, *141*, 8951–8968.

[28] L.-Y. Sung, C.-L. Chen, S.-Y. Lin, K.-C. Li, C.-L. Yeh, G.-Y. Chen, C.-Y. Lin, Y.-C. Hu, *Nat. Protoc.* **2014**, *9*, 1882–1899.

[29] G. S. Biggs, E. E. Cawood, A. Vuorinen, W. J. McCarthy, H. Wilders, I. G. Riziotis, A. J. van der Zouwen, J. Pettinger, L. Nightingale, P. Chen, A. J. Powell, D. House, S. J. Boulton, J. M. Skehel, K. Rittinger, J. T. Bush, *bioRxiv* **2024**, 2024.2007.2025.605137.

[30] J. Mason, H. Wilders, D. J. Fallon, R. P. Thomas, J. T. Bush, N. C. O. Tomkinson, F. Rianjongdee, *Digit. Discov.* **2023**, *2*, 1894–1899.

[31] N. Tanaka, K. Ohno, T. Niimi, A. Moritomo, K. Mori, M. Orita, *J. Chem. Inf. Model.* **2009**, *49*, 2677–2686.

[32] D. Rogers, M. Hahn, *J. Chem. Inf. Model.* **2010**, *50*, 742–754.

[33] B.-F. Krippendorff, R. Neuhaus, P. Lienau, A. Reichel, W. Huisinga, *J. Biomol. Screen.* **2009**, *14*, 913–923.

[34] Z. Jin, X. Du, Y. Xu, Y. Deng, M. Liu, Y. Zhao, B. Zhang, X. Li, L. Zhang, C. Peng, Y. Duan, J. Yu, L. Wang, K. Yang, F. Liu, R. Jiang, X. Yang, T. You, X. Liu, X. Yang, F. Bai, H. Liu, X. Liu, L. W. Guddat, W. Xu, G. Xiao, C. Qin, Z. Shi, H. Jiang, Z. Rao, H. Yang, *Nature* **2020**, *582*, 289–293.

[35] D. Yamane, R. Tetsukawa, N. Zenmyo, K. Tabata, Y. Yoshida, N. Matsunaga, N. Shindo, A. Ojida, *J. Med. Chem.* **2023**, *66*, 9130–9146.

[36] C. A. Nicolaou, I. A. Watson, H. Hu, J. Wang, *J. Chem. Inf. Model.* **2016**, *56*, 1253–1266.

[37] C. Yung-Chi, W. H. Prusoff, *Biochem. Pharmacol.* **1973**, *22*, 3099–3108.

[38] T. W. Johnson, R. A. Gallego, M. P. Edwards, *J. Med. Chem.* **2018**, *61*, 6401–6420.

[39] W. McCorkindale, M. Filep, N. London, A. A. Lee, E. King-Smith, *RSC Med. Chem.* **2024**, *15*, 1015–1021.

[40] a) Y. Yamauchi, S. Konno, N. Omura, N. Yoshioka, A. Hingst, M. Gütschow, C. E. Müller, A. Taguchi, A. Taniguchi, A. Kawaguchi, Y. Hayashi, *ACS Chem. Biol.* **2024**, *19*, 1028–1034; b) Y. Hirose, N. Shindo, M. Mori, S. Onitsuka, H. Isogai, R. Hamada, T. Hiramoto, J. Ochi, D. Takahashi, T. Ueda, J. M. M. Caaveiro, Y. Yoshida, S. Ohdo, N. Matsunaga, S. Toba, M. Sasaki, Y. Orba, H. Sawa, A. Sato, E. Kawanishi, A. Ojida, *J. Med. Chem.* **2022**, *65*, 13852–13865.

Manuscript received: September 23, 2024
Revised manuscript received: November 15, 2024
Accepted manuscript online: December 4, 2024
Version of record online: ■■, ■■

Forschungsartikel

Medicinal Chemistry

H. Wilders, G. Biggs, S. M. Rowe, E. E. Cawood, I. G. Riziotis, A. R. Rendina, E. K. Grant, J. Pettinger, D. J. Fallon, M. Skehel, D. House, N. C. O. Tomkinson, J. T. Bush* **e202418314**

Expedited SARS-CoV-2 Main Protease Inhibitor Discovery through Modular 'Direct-to-Biology' Screening

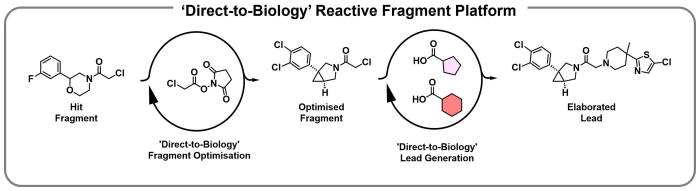

Direct-to-biology workflows promise to accelerate hit optimisation for drug discovery. Here, we describe a direct-to-biology method for the efficient synthesis and screening of cysteine-reactive fragments and its application in the optimisation of a micromolar inhibitor of SARS-CoV-2 main protease towards nanomolar covalent analogues. Additionally, we describe an under-reported switch from the covalent series to a potent, non-covalent series.